RSC Advances

ROYAL SOCIETY OF CHEMISTRY

www.rsc.org/advances

Cite this: DOI: 10.1039/c0xx00000x

www.rsc.org/xxxxxx

ARTICLE TYPE

Synthesis of amorphous porous zirconium phosphonate materials: tuneable from micropore to mesopore sizes

Xiu-Zhen Lin[a] and Zhong-Yong Yuan*[a]

Received (in XXX, XXX) Xth XXXXXXXXX 20XX, Accepted Xth XXXXXXXXX 20XX

DOI: 10.1039/b000000x

Amorphous porous zirconium phosphonate materials constructed from 1-hydroxyethylidene-1,1'-diphosphonic acid, having tunable from micropore to mesopore sizes, were hydrothermally synthesized in a CTAB-H_2O-ethanol ternary system (CTAB = cetyltrimethyl ammonium bromide). The as-synthesized materials were mesostructured, and could be transformed into (super-)microporous hybrid solids after surfactant-extracted process. By varying the hydrothermal time, the pore sizes of the obtained zirconium phosphonates could be efficiently tuned from micropore (0.87 nm) to mesopore (2.5 nm) range, and their micropore specific surface areas ranged from 116 to 509 m^2/g with the pore volumes in the range of 0.11–0.35 cm^3/g. To rationalize the formation of microporosity from mesostructure, a working hypothesis of 2-step condensation of Zr-OH groups with RP-OH species involving one step in mesostructured phase formation period and the other at surfactant removal process is proposed according to the XRD, TEM, FT-IR and XPS analysis of the samples before and after surfactant removal. Considering the acidity and tunable pore sizes, the prepared porous zirconium phosphonates may find their potential applications in adsorption, shape-selective heterogeneous catalysis, ion exchange and proton conduction.

1. Introduction

Metal organophosphonate with stable P-O-M and C-P bonds is a kind of organic-inorganic hybrid material with multifunctionality, exhibiting potential applications in catalysis, ion exchange, adsorption, photochemistry and so on.[1-7] In the past decades, quite a few crystalline metal phosphonates with small micropores (pore size < 1.0 nm) have been reported and used as adsorbents for gas molecules.[8-12] Also, several mesoporous metal organophosphonates with pore sizes of 2 – 10 nm and amorphous framework were synthesized by the surfactant templating.[13-17] However, much less attention was devoted to the synthesis of supermicroporous metal phosphonate materials with pore sizes of 1.0 – 2.0 nm, though the materials in this pore size range are greatly important because they bridge the gap between microporous zeolites and mesoporous materials.[18,19]

In fact, the past years have witnessed efforts devoted to generate supermicroporosity in metal phosphonates by using bisphosphonic acids [H_2O_3P-R-PO_3H_2; R = -$C_{12}H_8$- or -$C_6H_4OC_6H_4$-] as crosslinking agents or phenylphosphonic acids as single ligands.[20-22] Layered zirconium arylbisphophonates with ideal formula Zr[$O_3P(C_6H_4)_n$-PO_3] were reported, and their pore sizes could be adjusted in the range of 0.8 − 2 nm by adding different amounts of dimethyl sulfoxide, although their porosity was considered to originate from the interlayer spaces.[23] Clearfield and co-workers prepared a series of tin(IV) phosphonates with the pore sizes ranging from small micropore (0.9 nm) to mesopore (2.7 nm) range,[22] and the microporosity was justified as an inherent feature arising from the aggregation of nanorods into micro-sized spheres that contained tunnels of supermicropore dimensions. Layered porous tin(IV) phosphonophenoxyphenylphosphonates were synthesized by using the precursor 4-(4'-phosphonophenoxy)phenyl phosphonic acid and employing n-alcohol (C1-C6)-water mixtures in the presence of hydrofluoric acid,[21] and their pore sizes could be controllable in the range of 1.2 − 1.6 nm by the chain length of the alcohols. The microporous layered tin [24] and titanium [25] phenylphosphonates could also be synthesized in the presence of sodium dodecylsulfate. All the above mentioned porous metal organophosphonates were crystalline with aryl groups in the framework, and the generation of micropores in these materials obeyed different pathways.

In this paper, we developed a new synthetic route to prepare (super-)microporous zirconium organobisphosphonates with amorphous pore wall in the presence of surfactant cetyltrimethyl ammonium bromide (CTAB). Through a distinct CTAB-H_2O-ethanol system, a series of porous zirconium organobisphosphonates bridged with 1,1'-hydroxyethylidene groups instead of phenyl groups were obtained, and their pore sizes could be facilely tuned from 0.87 to 2.50 nm by controlling the hydrothermal time, accompanying with the micropore surface areas varying from 116 to 509 m^2/g. A rational hypothesis involving 2-step condensation was proposed to understand the fabrication of the supermicropores embedded within the products.

2. Experimental

2.1. Materials and synthesis

Zirconium oxychloride ($ZrOCl_2\ 8H_2O$) and cetyltrimethyl ammonium bromide (CTAB) were obtained from Tianjin Guangfu Chemical Co., and 1-hydroxy ethylidene-1,1'-diphosphonic acid (HEDP, 60 *wt*% aqueous solution) was from Henan Qingyuan Chemical Co. All chemicals were used as received without further purification.

Typically, 0.5 g of CTAB was added into an aqueous solution containing 1.72 g of HEDP, 4 ml of ethanol and 25 ml of H_2O at 45 ℃, and the obtained transparent solution was stirred for 2 h. A $ZrOCl_2$ solution (0.4 g of $ZrOCl_2$ dissolved in 5 ml of H_2O) was then added dropwise, and white precipitate produced immediately, which was further stirred overnight. The mixture was transferred into an autoclave to undergo hydrothermal treatment at 110 ℃ for a period of time (from 0 to 72 h). Afterward the white solid was collected by filtering, washing with water and drying under vacuum at 80 ℃ for 6 h. The surfactant was removed by stirring 1.0 g of the as-synthesized product, 150 ml of ethanol and 3.6 ml of 36 *wt*% HCl aqueous solution at 60 ℃ for 8 h. The obtained microporous zirconium organophosphonates were denoted as ZrHEDP-*x*, where *x* represented the hydrothermal time.

2.2. Characterization

The chemical compositions of Zr and P were analyzed by inductively coupled plasma (ICP) emission spectroscopy on a Thermo Jarrell-Ash ICP-9000 (N + M) spectrometer, and C, N and H were determined on a Vario-EL elemental analyzer. X-ray diffraction (XRD) patterns were recorded on a Bruker D8 Focus diffractometer with Cu K_α radiation operated at 40 kV and 40 mA. N_2 adsorption-desorption isotherms were obtained on a Quantachrome NOVA 2000e analyzer at liquid nitrogen temperature (77 K). The samples were degassed at 120 ℃ for 5 h prior to the measurement. The surface areas were measured by the multi-point Brunauer-Emmett-Teller (BET) method and the microporous surface areas were obtained by the DeBoer *t*-plot method. The pore size distributions were calculated by the quenched solid density functional theory (QSDFT) and the Saito-Foley (SF) method. Transmission electron microscopy (TEM) was carried out on a Philips Tecnai G20 operated at 200 kV. Fourier transform infrared (FT-IR) spectra were measured on a Bruker VECTOR 22 spectrometer with KBr pellet technique, and the ranges of spectrograms were 4000 to 400 cm^{-1}. X-ray photoelectron spectroscopy (XPS) measurements were performed on a Kratos Axis Ultra DLD (delay line detector) spectrometer equipped with a monochromatic Al-K_α X-ray source (1486.6 eV). Thermogravimetry (TG) and differential thermogravimetry (DTG) were performed on a TA SDT Q600 instrument at a heating rate of 10 ℃/min under N_2 atmosphere, using α-Al_2O_3 as the reference.

2.3. H^+ exchange capacity titration

0.1 g of sample was mixed with 20 ml of 10 *wt*% NaCl solution, and stirred at room temperature for 12 h, followed by centrifugation to recover the filtrate. Then the acidic content of the filtrate was determined by titration method with a 0.02 M NaOH solution.

3. Results and discussion

Fig. 1 shows the low-angle XRD patterns of as-synthesized and surfactant-removed ZrHEDP-*x* samples. As to the as-synthesized sample ZrHEDP-1 synthesized after hydrothermal treatment at 110 ℃ for 1 h, one main diffraction peak at 2.48 °(2θ) with one broad shoulder around 3.5 – 5.0 ° was observed. This main peak could be indexed as (1 0 0) reflection of hexagonal mesostructure, and the presence of broad shoulder peak indicates the formation of wormhole-like or some undefined poorly ordered mesostructure. When the hydrothermal time of the sample ZrHEDP-*x* increased to 2 – 24 h, the same diffractions were observed, excepting the shift of the (1 0 0) reflection towards lower 2θ angle to 2.35 °, implying the expanding of mesostructure with the hydrothermal time. The shift of main reflection to lower 2θ angle for ZrHEDP-*x* might be induced by the motion of ethanol from aqueous solution to surfactant-formed micelle, leading to the enlargement of micelle volume.[26] However, after acid extraction, the diffraction patterns of those samples synthesized under different hydrothermal time were totally different. No obvious diffraction peaks were observed for ZrHEDP-1, showing the complete collapse of its mesostructure; and ZrHEDP-2 left one single broad peak in the range of 1 − 4 °, suggesting the presence of porosity from the regularly aggregation of nanoparticles;[27] while, a relatively strong and sharp peak maintained for ZrHEDP-24, although its relative intensity was much lower than its as-synthesized counterpart. When extending the hydrothermal time to 72 h, ZrHEDP-72 sample displayed similar profile as that of ZrHEDP-24 both before and after surfactant removal (not shown here). This reflects that the mesostructure of ZrHEDP-*x* samples was susceptible to collapse during surfactant-removed process and the hydrothermal treatment time played a crucial role in improving the mesostructure stability. Besides, only one broad peak in the wide angle for those mesostructured samples was shown, displaying the amorphous nature of the pore wall for ZrHEDP-*x* samples (Fig. S1 in Supporting Information).

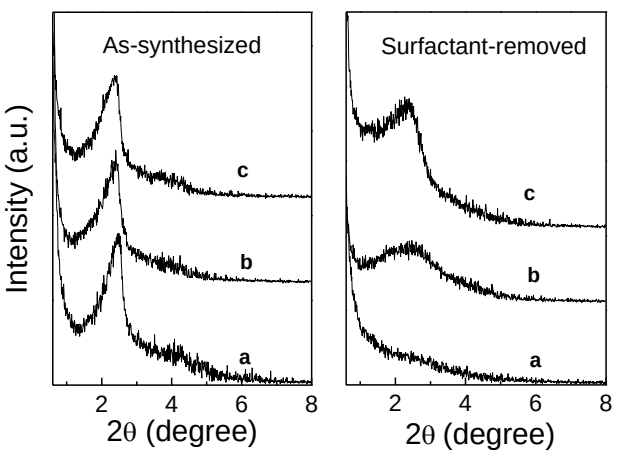

Fig. 1 Low-angle XRD patterns of as-synthesized (*left*) and acid-extracted (*right*) ZrHEDP-*x* synthesized at 110 ℃ with different aging time: (a) 1 h, (b) 2 h and (c) 24 h.

TEM images of ZrHEDP-1 and ZrHEDP-24 before and after surfactant removal are shown in Fig. 2. For the as-synthesized ZrHEDP-1 and ZrHEDP-24 samples that contained surfactant species, as shown in Figs. 2A and 2C respectively, wormhole-like mesostructures were clearly presented, besides striped patterns in some domains, revealing their partial ordering of the porous structure. After surfactant removal, no ordered mesostructure was

observed for these two samples but wormhole-like pores in the microporous range presented (Figs. 2B and 2D). The TEM results were consistent with that obtained from XRD, showing the deterioration of mesostructure after surfactant removal.

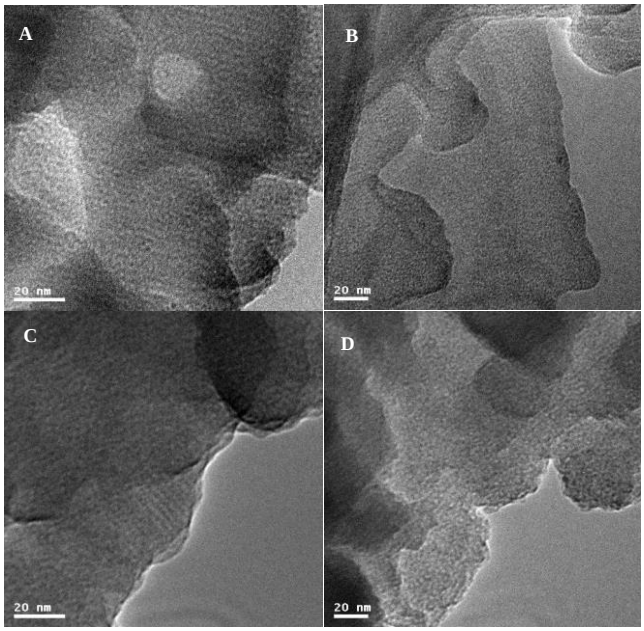

Fig. 2 TEM images of ZrHEDP-1 before (A) and after (B) surfactant removal, and ZrHEDP-24 before (C) and after (D) surfactant removal.

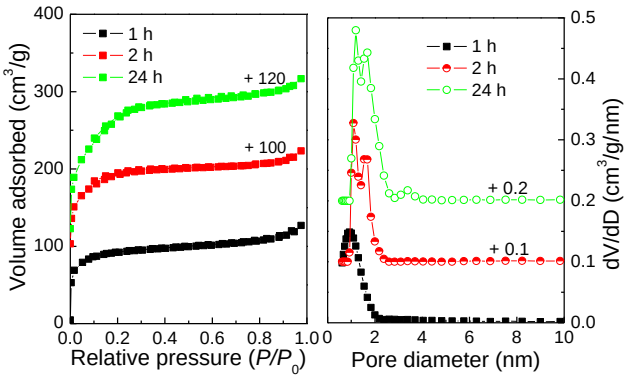

Fig. 3 N_2 adsorption-desorption isotherms of ZrHEDP-*x* samples with different hydrothermal periods (*left*), with their corresponding pore size distributions (*right*).

The N_2 adsorption-desorption is a reliable technique to obtain effective information about the pore structure of solid materials. Fig. 3*left* shows the N_2 adsorption-desorption isotherms of ZrHEDP-*x* samples after surfactant removal. The sample ZrHEDP-1 presented the typical type I isotherms, exhibiting an increase in the volume of adsorbed nitrogen at the relative pressure $P/P_0 < 0.1$ and then leveling off. Such a behavior is usually associated with adsorption in micropores.[28] The samples ZrHEDP-2 and ZrHEDP-24 exhibited isotherms of a transitional type between type I and IV, suggestive of the pore sizes between micropore and mesopore ranges. And no clear presence of hysteresis loops indicates no slit-like pores from nanoparticle aggregate and no obvious pore-blocking effect from narrow pores during desorption.[29] In comparison with ZrHEDP-1, a pronounced nitrogen uptake for ZrHEDP-2 and ZrHEDP-24 shifted downward and leveled off at relative pressures $P/P_0 = 0.2$ and 0.26 respectively, implying the enlargement of pore size for the present materials. The corresponding pore size distributions (PSD) calculated by the QSDFT model are shown in Fig. 3*right*. ZrHEDP-1 exhibited narrow PSD centered at about 0.87 nm in the range of typical microporous domain. The PSD of ZrHEDP-2 shows two peaks centered at 1.05 and 1.57 nm. For ZrHEDP-24, two main peaks centered at 1.15 and 1.65 nm along with a weak shoulder in the mesoporous range with a pore size at 3.5 nm were presented. It was noteworthy that the pore size for ZrHEDP-2 and ZrHEDP-24 was in the range of supermicropore (a pore size in the range of 1−2 nm). Therefore, with the increase of the hydrothermal treatment time, the pore size of ZrHEDP-*x* progressively enlarged. The BET surface areas of 345, 350 and 561 m^2/g with pore volumes of 0.10, 0.19 and 0.30 cm^3/g are obtained for ZrHEDP-1, ZrHEDP-2 and ZrHEDP-24, respectively, including a considerable microporous surface area in the range of 259−305 m^2/g (Table 1).

The inorganic and organic compositions of the porous zirconium phosphonate hybrid ZrHEDP-24 were investigated by ICP technique and CHN analysis, which is taken as being representative. For the as-synthesized ZrHEDP-24, P/Zr molar ratio in the hybrid framework was 3.42 (10.74% for P and 8.29% for Zr in mass). The carbon, hydrogen, and nitrogen contents were 32.76, 7.43 and 1.45 mass%, respectively. According to the elemental analyses, the formula of the as-synthesized material can be described as $Zr(O_3PCOH(CH_3)PO_3)_{1.71} \cdot 1.23C_{16}TA^+ \cdot 10.7H_2O$, and OH^- species such as terminal Zr-OH would be required for charge balance. After surfactant removal, no nitrogen atoms were detected in the acid-extracted ZrHEDP-24 by CHN analysis, revealing that almost all of the $C_{16}TA^+$ cations were removed by acidic ethanol extraction method.

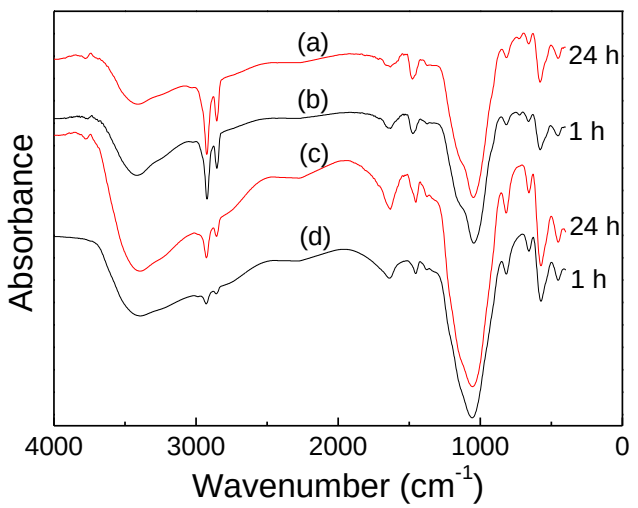

Fig. 4 FT-IR spectra of as-synthesized (a) ZrHEDP-24 and (b) ZrHEDP-1, and acid-extracted (c) ZrHEDP-24 and (d) ZrHEDP-1.

Cite this: DOI: 10.1039/c0xx00000x

www.rsc.org/xxxxxx

ARTICLE TYPE

Table 1 Textural parameters and H^+ exchange capacities for ZrHEDP-*x* samples prepared under various aging times.

Sample	Aging time (h)	S_{BET} [a] (m^2/g)	S_{micro} [b] (m^2/g)	V_{pore} [c] (cm^3/g)	D_{DFT} [d] (nm)	D_{SF} [e] (nm)	$C_{H^+\ exchange}$ (mmol/g)
ZrHEDP-1 [f]	1	17	—	0.04	—	—	1.38
ZrHEDP-24 [f]	24	74	—	0.24	—	—	1.06
ZrHEDP-0	0	164	116	0.11	1.54	1.50	1.72
ZrHEDP-1	1	345	259	0.20	0.87	1.11	1.59
ZrHEDP-2	2	350	202	0.19	1.05, 1.57	1.09, 1.73	1.60
ZrHEDP-24	24	561	305	0.30	1.15, 1.65	1.11, 1.70	1.38
ZrHEDP-72	72	622	509	0.35	1.20, 1.38-2.50	1.11, 1.74	1.36

[a] The specific surface area calculated from the linear part of the BET plot. [b] Calculated by the *t*-plot method. [c] Total pore volume, taken from the volume of N_2 adsorbed at $P/P_0 = 0.97$. [d] Pore diameter obtained from the maxima of the pore size distribution curve calculated by the QSDFT model. [e] The pore size calculated by the SF method. [f] Synthesized without the addition of ethanol in the synthetic condition.

Table 2 Positions of binding energy and relative percent (%) of four components $O_{C\text{-}O}$ (I), $O_{P\text{-}O\text{-}H}$ (II), $O_{P\text{-}O\text{-}Zr}$ (III) and $O_{Zr\text{-}O\text{-}Zr}$ (IV) in XPS O1s spectra for ZrHEDP-1 and ZrHEDP-24 samples, both before and after surfactant removal.

Samples	Binding Energy [a] (eV)				O_{1s} component [b] (%)		
	I	II	III	IV	II	III	II/III
as-synthesized ZrHEDP-1	533.0	531.95	531.16	530.45	33.3	46.3	0.72
acid-extracted ZrHEDP-1	533.19	532.43	531.58	530.99	24.8	62.7	0.40
as-synthesized ZrHEDP-24	533.22	532.05	531.0	530.27	27.1	52.4	0.52
acid-extracted ZrHEDP-24	533.33	532.50	531.61	530.84	22.7	67.3	0.34

[a] Binding energy based on XPS O 1s line. [b] Atomic relative percent calculated from relative peak area in XPS O 1s line.

The FT-IR spectra of ZrHEDP-1 and ZrHEDP-24 before and after surfactant removal are shown in Fig. 4. Before surfactant removal, a broad band with maximum at 3400 cm^{-1} and a sharp peak at 1646 cm^{-1} were observed (Figs. 4a and 4b), which can be attributed to OH groups and physically adsorbed water.[30] Two sharp bands at 2928 and 2854 cm^{-1} are attributed to C-H stretching vibration from CTAB and organophosphonate groups. A band at 1462 cm^{-1} and a weak band at 1382 cm^{-1}, ascribed to C-P and C-O stretching vibration respectively, were both from organophosphonate groups.[31] The sharp and broad band at 1055 cm^{-1} is assigned to PO_2 symmetrical stretching vibration.[32] The shoulder band at 1150 cm^{-1} is ascribed to P-O asymmetrical stretching vibration,[33] demonstrating the presence of P-O vibration from uncomplexed RP-OH groups in as-prepared samples. After surfactant removal (Figs. 4c and 4d), all the absorption bands remained in surfactant-extracted samples, but the intensity in band strength for some peaks changed in comparison with surfactant-contained samples. The weakening in the absorption bands for C-H stretching vibration (2928 and 2854 cm^{-1}) together with the relative intensity increasing from C-P (1462 cm^{-1}) and C-O (1382 cm^{-1}) groups demonstrated the removal of surfactant with the maintenance of organophosphonate groups in the hybrid framework. Besides, the weakening of the band from P-O (1150 cm^{-1}) vibration in uncomplexed RP-OH groups suggested the further condensation of RP-OH species within the hybrid framework during surfactant removal process. From the FT-IR analysis, it is thus revealed the integrity of organic species from phosphonate groups in the surfactant-removed samples.

High-resolution XPS analysis is a powerful technique to study the atomic bonding and coordinated environment of elements for solid materials and gives information about the relative content of the analyzed element up to *ca*. 5 nm in depth. The surface atomic concentration was 6.21% for P and 1.82 % for Zr in the as-synthesized ZrHEDP-24, giving a P/Zr molar ratio of 3.41. This value is almost consistent with the data from the elemental analysis (3.42), suggesting the compositional homogeneity throughout the hybrid material.

Fig. 5 displays the XPS spectra of the O 1s taken on the surfaces of as-synthesized and surfactant-removed ZrHEDP-1 and ZrHEDP-24 samples. For all the spectra, the O 1s line might be fitted by four components. The highest E_b component (peak I) at ~533.0 eV was contributed from C-O bond. The second E_b component (peak II) at ~532.0 eV may be assigned to phosphonate P-O-H groups (actually $P\text{-}O^- \cdots CTA^+$ species should be present instead of P-O-H for the sample before surfactant removal). The main peak (peak III) at ~531.5 eV was mostly attributed to Zr-O-P interactions,[34] but other contributions such as P=O and Zr-O from Zr-OH were also possible.[35] The most important feature was the presence of a lowest E_b component (peak IV) at ~530.3 eV, characteristic of oxide Zr-O interactions,[34,36] which suggests that there was a very small part

of ZrO_2 oligomer present in the hybrid framework and most part was homogeneously distributed with P-O-Zr bonds.

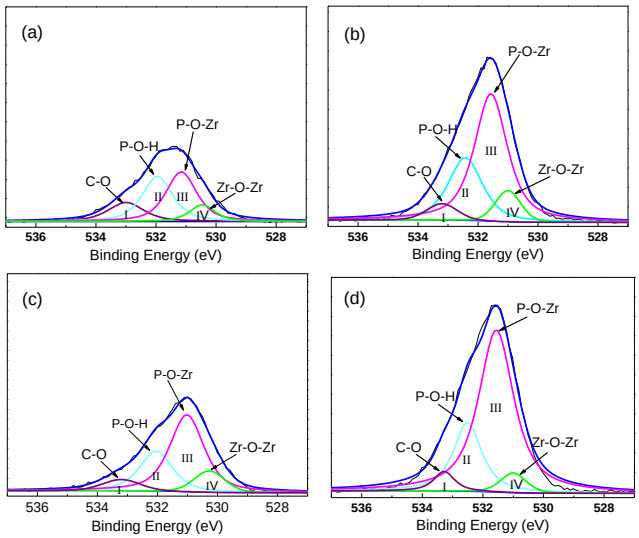

Fig. 5 XPS O 1s spectra of ZrHEDP-1 before (a) and after (b) surfactant removal, and ZrHEDP-24 before (c) and after (d) surfactant removal. Fitting peaks I, II, III and IV resulted from signal deconvolution.

Moreover, a careful look can find that the binding energies of O 1s for zirconium organophosphonate samples before and after surfactant removal were distinguishing, which are summarized in detail in Table 2. In comparison with the as-synthesized samples, the O 1s peaks shifted towards higher binding energies after acid-extraction of the samples. The similar shift of the binding energies between the as-synthesized and surfactant-free samples was also observed for Zr 3s and P 3p lines (Figs. S2 and S3 in Supporting Information). Thus, such a shift of binding energy for O 1s, Zr 3s and P 3p of the samples before and after surfactant removal should be caused by the surfactant.

In addition, the relative percent of O 1s species in the hybrid framework before and after surfactant removal also changed, as summarized in Table 2. As to the sample ZrHEDP-1, after surfactant removal, the relative percent of $O_{P\text{-}O\text{-}Zr}$ increased from 46.3% to 62.7%, and $O_{P\text{-}O\text{-}H}$ decreased from 33.3 % to 24.8 %. While for the ZrHEDP-24, the relative percent of $O_{P\text{-}O\text{-}Zr}$ increased from 52.4 % to 67.3 %, and $O_{P\text{-}O\text{-}H}$ decreased from 27.1 % to 22.7 % after surfactant removal. It is reasonable to understand this evolution in terms of the continuing condensation of residual P-OH with Zr-OH species on the pore wall to form P-O-Zr bond during the acid-extraction process to remove surfactant. On the other hand, the ratio of $O_{P\text{-}O\text{-}H}$ to $O_{P\text{-}O\text{-}Zr}$ for the as-synthesized ZrHEDP-1 is 0.72, which is higher than that of the as-synthesized ZrHEDP-24 (0.52), reflecting a significant increase in the polymerization degree of hybrid framework by extending hydrothermal time. Besides, the $O_{P\text{-}O\text{-}H}$ species leftover on the ZrHEDP-*x* samples after surfactant removal can act as the acid provider and should be responsible for the significant hydrogen ion exchange capacity, as shown in Table 1. Indeed, all the samples had moderately high H^+ exchange capacity in the range of 1.36–1.72 mmol/g (Table 1). This suggests that the synthesized zirconium organophosphonate materials having tunable pore sizes from small micropore to supermicropore range with significant BET surface area and H^+ ion exchange capacity may find potential applications including separation and acid catalysis.

Fig. 6 gives TG-DTG curves of the as-synthesized ZrHEDP-1 and ZrHEDP-24 samples. In the TG curves, the first weight loss stage from room temperature to 220 ℃ could be ascribed to the desorption of the physically adsorbed water and ethanol. The weight loss of ~29 % in the region of 220 – 380 ℃ is attributed to the decomposition of the surfactant, and the weight loss of about 10.5 % from 380 to 480 ℃ is due to the decomposition of organophosphonate. The last stage in the range of 480 – 600 ℃ is attributed to the further combustion of residual coke from surfactant and organophosphonate. It is thus revealed that the hybrid framework of the surfactant-contained zirconium organophosphonates can be thermally stable up to 380 ℃.

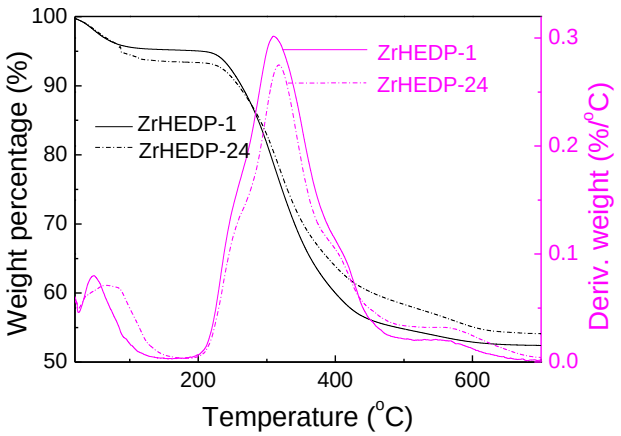

Fig. 6 TG-DTG curves of as-synthesized ZrHEDP-1 and ZrHEDP-24 samples.

In the preparation of ZrHEDP-*x*, $ZrOCl_2$ aqueous solution was dropwise added into the HEDP-CTAB-ethanol-H_2O mixed solution, followed by hydrothermal treatment of the mixture, resulting in the formation of mesophase. Herein, CTAB played a structure directing role in the formation of mesostructure. The acidic ethanol solution can be utilized to successfully extract the surfactant imbedded in the hybrid materials, while the extraction with pure ethanol was inefficient to remove the CTAB molecules. It thus can be postulated that the acidic ethanol extraction procedure for surfactant removal underwent an ionic exchange process possibly by replacement of CTA^+ cations with H^+ ions in order to keep the charge balance of the hybrid framework. Primarily, the CTA^+ cations embedded in the hybrid sample might electrostatically interact with anionic species in the hybrid framework, such as $RP\text{-}O^-$ and $Zr\text{-}O^-$, in the form of $RP\text{-}O^- \cdots CTA^+$ and $Zr\text{-}O^- \cdots CTA^+$ species, and these species were replaced by RP-O-H and Zr-O-H groups after acidic extraction. Comparing the samples before and after surfactant removal, one can find that the chemical environment of oxygen species connected to organophosphorus or zirconium changed. This transformation should be responsible for the shift of binding energy of O 1s, as well as Zr 3s and P 3p for ZrHEDP-1 and ZrHEDP-24 samples before and after surfactant removal, as seen from the XPS spectra in Fig. 5, Figs. S2 and S3.

In order to understand the influences of synthetic parameters on the varying of pore sizes and mesostructure stability of the final products, different synthetic conditions were undertaken.

Without the addition of CTAB during the synthesis, white solid xerogel with poor textural properties was obtained. When CTAB was used as template but no ethanol was added in the synthetic system, no low-angle XRD peaks were observed on the corresponding final samples, and the nitrogen adsorption-desorption isotherms indicated their poor textures (Table 1), with a very low BET surface area of 17 and 74 m^2/g for the products hydrothermally treated for 1 and 24 h, respectively, giving wide-spread pore size distributions. In contrast, the addition of 4 ml of ethanol in the synthetic mixture led to the formation of mesostructure with excellent textural properties: total BET surface areas in the range of 345−561 m^2/g with microporous BET surface areas from 259−305 m^2/g, together with narrow pore size distributions, upon varying hydrothermal treatment time from 1 to 24 h. The formation of mesostructure in the presence of ethanol is most likely through a cooperative condensation of surfactants and zirconium organophosphonates. From the thermodynamic point of view, the formation of mesostructure can be roughly divided into two steps, namely the formation of micelles and then their condensation. At the first step, it includes the charge density matching between the surfactant and the inorganic precursor, which is essential, or else phase separation would occur. When the ethanol was not added in the synthetic system, phase separation between the micelles and the zirconium organophosphonate nanoparticles should dominate, because of the strong repulsion between micelles and hybrid nanoparticles, leading to the charge density mismatching, and no mesostructure formed. Upon the addition of ethanol, the alcohol molecules penetrated into the micelle, leading to an expansion of micelle volume, which effectively minimizes the Coulombic repulsion between the head groups of surfactants, as well as reducing the repulsion between micelles and hybrid nanoparticles; and thus micelle-hybrid nanoparticle composites came into being, together with their further condensation to form mesostructure. The effects of alcohol additives as cosolvent or cosurfactant on the structural ordering have been reported for mesostructured silica materials.[26,37-39] And this method was demonstrated to be an efficient and feasible way to adjust the pore sizes and control the mesophase formation. In this work, ethanol played a role as cosurfactant in assisting the formation of zirconium organophosphonate mesostructures.

In the presence of ethanol, if the precursor mixture was stirred at 45 ℃ overnight and then directly filtrated and dried without further hydrothermal treatment at 110 ℃, the resultant solids was not mesostructured but with a microporous surface area of only 116 m^2/g. This is because the penetration of ethanol inside micelle did not occur at relatively low temperature and a high temperature like 110 ℃ was needed to provide hydrophobic driving force.[40] After hydrothermal treatment at 110 ℃ for 1 h, zirconium organophosphonate mesostructure was formed. By extending the hydrothermal treatment time, a shift of (1 0 0) peak towards lower 2θ angle for ZrHEDP-*x* samples took place (Fig. 1*left*). The continuing penetration of ethanol molecules from aqueous solution into micelles with hydrothermal treatment time prolonging should be responsible for a gradual expansion of micelle volume. After acid extraction of the resultant solids, the mesostructure for ZrHEDP-1 completely collapsed, while a single broad peak left for ZrHEDP-2, and a relatively single and strong peak preserved for ZrHEDP-4 (Fig. 1*right*), accompanying with the varying of pore sizes from micropore to mesopore range. This phenomenon should be associated with the condensation degree of hybrid framework to different extent, as well as the shrinkage of mesostructure during surfactant removal process, as revealed by the XPS analysis of ZrHEDP-*x* samples before and after surfactant removal (Table 2). For the ZrHEDP-1, after surfactant removal, the oxygen species of $O_{P\text{-}O\text{-}H}$ decreased from 33.3 % to 24.8 %, accompanying with the increase of $O_{P\text{-}O\text{-}Zr}$ from 46.3 % to 62.7 %, suggesting the condensation of organophosphorus species in the hybrid framework. The same case happened on ZrHEDP-24 before and after surfactant removal. The incomplete condensation of hybrid framework for surfactant-contained samples underwent further polymerization upon surfactant removal, and resulted in the mesostructure destruction, as revealed by the XRD patterns in Fig. 1 and TEM images in Fig. 2. What's different is that the difference in the value of $O_{P\text{-}O\text{-}H}/O_{P\text{-}O\text{-}Zr}$ for ZrHEDP-1 before and after surfactant removal was 0.32, and for ZrHEDP-24 was 0.18. This means that, during surfactant removal process, the polymerization degree of hybrid framework for ZrHEDP-1 was more significant than that of ZrHEDP-24. Thus different destruction degree for mesostructure triggered for ZrHEDP-1 and ZrHEDP-24. Correspondingly, by further extending the hydrothermal time, ZrHEDP-72 showed a better mesostructure. Also, the pore size increased from small micropore (0.87 nm for ZrHEDP-1) to supermicropore (1.15 and 1.65 nm for ZrHEDP-24) and then to mesopore (1.38−2.5 nm for ZrHEDP-72) range, depending on the mesotructure destruction degree.

Herein, a possible 2-step condensation route was proposed for the formation of microporosity of zirconium organophosphonate with its mesostructured phase as the intermediate state, as shown in Fig. 7. The first step was in the material synthesis period. At the starting of material synthesis process, as soon as zirconium source was added into the solution of the HEDP-CTAB-contained mixture, the condensation of zirconium organophosphonate nanoparticles around surfactant micelles occured. During the polymerization, electrostatical interaction of either $Zr\text{-}O^-$ or $RP\text{-}O^-$ species with CTA^+ cations existed, which impeded the further condensation of the active species presented in the interface. Besides, there were still many Zr-OH and RPOH species left in the hybrid framework. As a result, Zr-OH and RPOH species both on the interface of surfactant and hybrid framework wall, as well as in the hybrid framework, were existent. Under hydrothermal treatment at 110 ℃, the further condensation of inorganic Zr-OH and organic RP-OH species in the hybrid framework happened, though it still was greatly incomplete. When the surfactant embedded in ZrHEDP-*x* was extracted by HCl/ethanol solvent, Zr-OH and RP-OH species were produced and the second step condensation occured. As a result, the shrinking of hybrid framework took place, accompanying with the collapse of mesostructure (proved by XRD in Fig.1). Therefore, rich microporosity was obtained after ZrHEDP-*x* was dried in vacuum.

Cite this: DOI: 10.1039/c0xx00000x

www.rsc.org/xxxxxx

ARTICLE TYPE

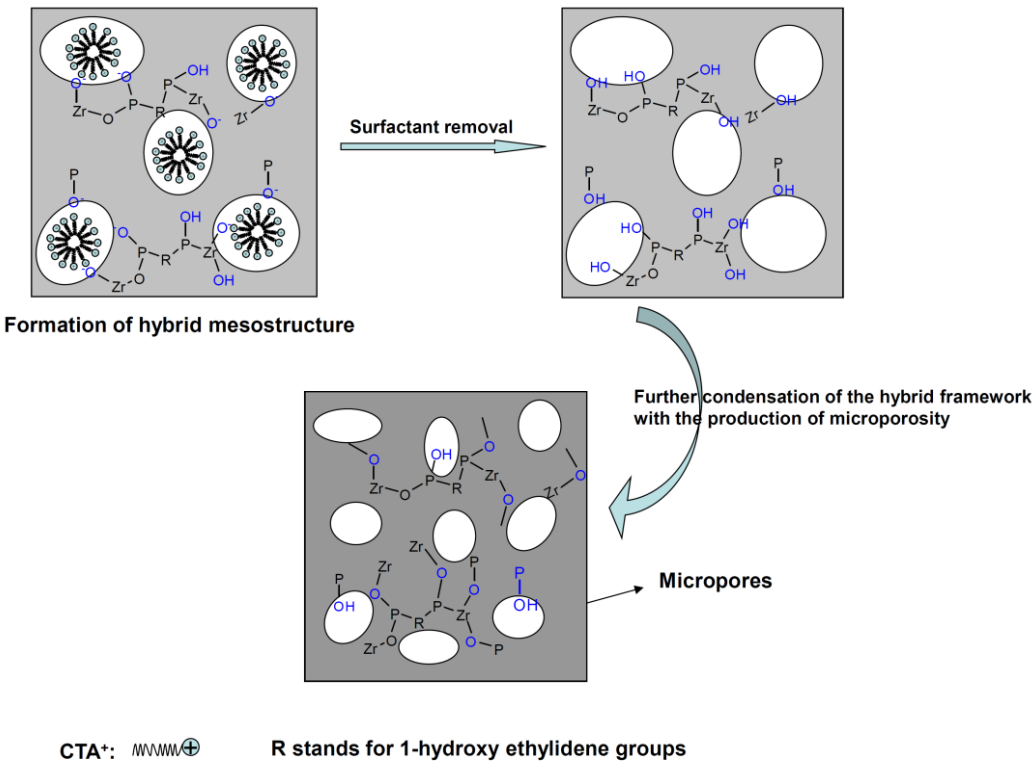

Fig. 7 A proposed microporous formation route for porous zirconium organophosphonate bridged with 1-hydroxyethylidene groups evolved from its mesostructured phase.

This synthetic route via the mesostructure formation as the intermediate state to synthesize (super-)microporous zirconium organodiphosphonates is quite different from the previous reported methods [20-25] that were either through the organic solvent (such as DMSO), by the nature of metal (Sn) or small surfactant as single template (SDS) to synthesize supermicroporous metal organophosphonates. Actually, the large degree of shrinkage of mesostructure for silica materials during surfactant template removal via calcination was well documented through the further condensation of Si-OH species at high temperature, and the pore size diameter could be obtained only close to 2 nm and difficult to be smaller.[41,42] Such small pore sizes in the region of 0.87 to 1.65 nm for the synthesized zirconium organophosphonate materials are not only related to the further condensation of hybrid framework at surfactant removal process, but also closely related with the controlled hydrothermal time as well as the innate nature of zirconium organophosphonate materials.

4. Conclusions

(Super-)microporous zirconium phosphonates with amorphous pore wall and 1-hydroxyethylidene groups bridged in the hybrid framework have been synthesized in the H_2O-ethanol-CTAB ternary system. The pore sizes of the obtained hybrids can be efficiently tuned from small micropore (0.87 nm) to mesopore (2.50 nm) range, depending on the hydrothermal time. And a significant microporous surface area from 116 to 509 m^2/g with high H^+ exchange capacity of 1.36–1.72 mmol/g was obtained. It was found that ethanol functioned as cosurfactant for the mesostructure formation by achieving the charge density matching between the surfactant and hybrid nanoparticles. Given the adjustability of pore sizes and the very nature of acidity, the synthesized (super-)microporous zirconium phosphonate hybrids should be significant for applications in separation, adsorption and shape selective heterogeneous catalysis.

Acknowledgements

This work was supported by the National Natural Science Foundation of China (21073099), the Specialized Research Fund for the Doctoral Program of Higher Education (20110031110016), the MOE Innovative Team (IRT13022), the 111 project (B12015), and the Key Laboratory of Advanced Catalytic Materials in Zhejiang Normal University (ZJHX201301).

Notes and references

[a] *Key Laboratory of Advanced Energy Materials Chemistry (Ministry of Education), Collaborative Innovation Center of Chemical Science and Engineering (Tianjin), College of Chemistry, Nankai University, Tianjin 300071, China. Fax: +86-22-23502604; Tel: +86-22-23509610; E-mail: zyyuan@nankai.edu.cn*

† Electronic Supplementary Information (ESI) available: [Wide-angle XRD patterns and XPS Zr 3s and P 3p spectra of the samples]. See DOI: 10.1039/b000000x/

1 G. Cao, H. Hong and T. E. Mallouk, *Acc. Chem. Res.*, 1992, **25**, 420–427.
2 P. Dutta, *Nature*, 1992, **358**, 621–621.
3 E. Stein, A. Clearfield and M. A. Subramanian, *Solid State Ionics*, 1996, **83**, 113-124.
4 A. Clearfield, *Curr. Opin. Solid State Mater. Sci.*, 1996, **1**, 268-278.
5 B. Bujoli, S.M. Lane, G. Nonglaton, M. Pipelier, J. Léger, D. R. Talham and C. Tellier, *Chem. Eur. J.*, 2005, **11**, 1980.
6 J. A. Groves, S. R. Miller, S. J. Warrender, C. Mellot-Draznieks, P. Lightfoot and P. A. Wright, *Chem. Commun.*, 2006, 3305.
7 Y. P. Zhu, T. Z. Ren and Z. Y. Yuan, *New J. Chem.*, 2014, **38**, 1905-1922.
8 Y. P. Zhu, T. Y. Ma, Y. L. Liu, T. Z. Ren and Z. Y. Yuan, *Inorg. Chem. Front.*, 2014, **1**, 360-383.
9 G. B. Hix, A. Turner, B. M. Kariuki, M. Tremayne and E. J. MacLean, *J. Mater. Chem.*, 2002, **12**, 3220–3227.
10 J. Li, L. Meng, Z. G. Sun, Z. M. Liu,Y. Zhao, J. Zhang, Y. Y. Zhu, X. Lu, L. Liu and N. Zhang, *Inorg. Chem. Commun.*, 2008, **11**, 211–214.
11 C. Serre, J. A. Groves, P. Lightfoot, A. M. Z. Slawin, P. A. Wright, N.Stock, T. Bein, M. Haouas, F. Taulelle and G. Fʹerey, *Chem. Mater.*, 2006, **18**, 1451.
12 K. Maeda, Y. Kiyozumi and F. Mizukami, *J. Phys. Chem. B*, 1997, **101**, 4402-4412.
13 T. Kimura, *Chem. Mater.*, 2005, **17**, 337-344.
14 T. Y. Ma and Z. Y. Yuan, *Chem. Commun.*, 2010, **46**, 2325–2327.
15 X. Shi, J. Yang and Q. H. Yang, *Eur. J. Inorg. Chem.*, 2006, 1936–1939.
16 X. Z. Lin and Z. Y. Yuan, *Eur. J. Inorg. Chem.*, 2012, 2661-2664.
17 M. V. Vasylyev, E. J. Wachtel, R. Popovitz-Biro and R. Neumann, *Chem. Eur. J.*, 2006, **12**, 3507–3514.
18 G. L. Zhao, Z. Y. Yuan and T. H. Chen, *Mater. Res. Bull.*, 2005, **40**, 1922-1928.
19 Z. Y. Yuan, W. Zhout and L.-M. Peng, *Chem. Lett.*, 2000, **29**, 1150-1151.
20 A. Bhaumik and S. Inagaki, *J. Am. Chem. Soc.*, 2001, **123**, 691.
21 M. M. Gómez-Alcántara, A. Cabeza, P. Olivera-Pastor, F. Fernández-Moreno, I. Sobrados, J. Sanz, R. E. Morris, A. Clearfield and M. A. G. Aranda, *Dalton Trans.*, 2007, 2394–2404.
22 A. Subbiah, D. Pyle, A. Rowland, J. Huang, R. A. Narayana, P. Thiyagarajan, J. Zoń and A. Clearfield, *J. Am. Chem. Soc.*, 2005, **127**, 10826-10827.
23 Z. K. Wang, J. M. Heisng and A. Clearfield, *J. Am. Chem. Soc.*, 2003, **125**, 10375-10383.
24 N. K. Mal, M. Fujiwara, Y. Yamada and M. Matsukata, *Chem. Lett.*, 2003, **32**, 292-293.
25 N. K. Mal, M. Fujiwara, Y. Yamada, K. Kuraoka and M. Matsukata, *J. Ceram. Soc. Jpn.*, 2003, **111**, 219-221.
26 H. P. Lin, Y. R. Cheng, S. B. Liu and C. Y. Mou, *J. Mater. Chem.*, 1999, **9**, 1197-1201.
27 A. Vantomme, Z. Y.Yuan and B. L. Su, *New J. Chem.*, 2004, **28**, 1083-1085.
28 M. Kruk and M. Jaroniec, *Chem. Mater.*, 2001, **13**, 3169-3183.
29 Y. Zhou and M. Antonietti, *Chem. Mater.*, 2004, **16**, 544-550.
30 T. Z. Ren, Z. Y. Yuan and B. L. Su, *Chem. Phys. Lett.*, 2003, **374**, 170.
31 X. J. Zhang, T. Y. Ma and Z. Y. Yuan, *Eur. J. Inorg. Chem.*, 2008, 2721-2726.
32 E. V. Bakhmutova-Albert, N. Bestaoui, V. I. Bakhmutov, A. Clearfield, A. V. Rodriguez and R. Llavona, *Inorg. Chem.*, 2004, **43**, 1264-1272.
33 F. Odobel, B. Bujoli and D. Massiot, *Chem. Mater.*, 2001, **13**, 163-173.
34 A. Cabeza, M. M. Gómez-Alcántara, P. Olivera-Pastor, I. Sobrados, J. Sanz, B. Xiao, R. E. Morris, A. Clearfield and M. A. G. Aranda, *Micropor. Mesopor. Mater.*, 2008, **114**, 322-336.
35 B. Adolphi, E. Jähne, G. Busch and X. Cai, *Anal. Bioanal. Chem.*, 2004, **379**, 646.
36 G. S. Herman, E. P. McDaniel and S. A. Joyce, *J. Electron Spectrosc.*, 1999, **101-103**, 433-438.
37 S. Q. Liu, P. Cool, O. Collart, P. Van Der Voort, E. F. Vansant, O. I. Lebedev, G. Van Tendeloo and M. H. Jiang, *J. Phys. Chem. B*, 2003, **107**, 10405-10411.
38 G. D. Zhang, X. Chen, Y. Zhao, Y. Z. Xie and H. Y. Qiu, *J. Phys. Chem. B*, 2007, **111**, 11708-11713.
39 W. Q. Wang, J. G. Wang, P. C. Sun, D. T. Ding and T. H. Chen, *J. Colloid. Interface Sci.*, 2009, **331**, 156-162.
40 H. M. Kao, C. C. Cheng, C. C. Ting and L. Y. Hwang, *J. Mater. Chem.*, 2005, **15**, 2989-2992.
41 M. Ogawa, *Chem. Commun.*, 1996, 1149-1050.
42 M. Ogawa and T. Kikuchi, *Adv. Mater.*, 1998, **10**, 1077-1080.

Synthesis of amorphous porous zirconium phosphonate materials: tuneable from micropore to mesopore sizes

Xiu-Zhen Lin and Zhong-Yong Yuan*

Table of Content

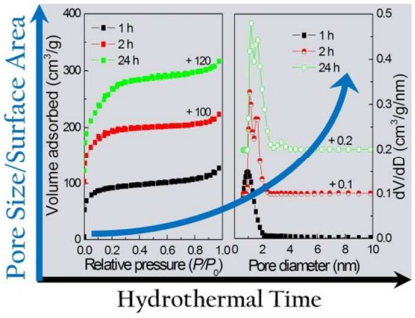

Amorphous super-microporous zirconium phosphonates with tunable pore size distributions were hydrothermally synthesized in a CTAB-H_2O-ethanol system by controlling the aging time.